

Article

The Role of $\alpha 3\beta 1$ Integrin Modulation on Fabry Disease Podocyte Injury and Kidney Impairment

Bruna Bosquetti ¹, Aline Aparecida Santana ¹ , Paulo César Gregório ¹, Regiane Stafim da Cunha ¹ ,
Guilherme Miniskosky ¹ , Julia Budag ¹, Célia Regina Cavichiolo Franco ¹, Edneia Amancio de Souza Ramos ¹ ,
Fellype Carvalho Barreto ²  and Andréa Emilia Marques Stinghen ^{1,*} 

- ¹ Experimental Nephrology Laboratory, Basic Pathology Department, Universidade Federal do Paraná, Curitiba 81531-980, Brazil; brubosquetti@gmail.com (B.B.); aline07santana@gmail.com (A.A.S.); paulocezargregorio@gmail.com (P.C.G.); regidacunha@ufpr.br (R.S.d.C.); gui.miniski@gmail.com (G.M.); jbudag98@gmail.com (J.B.); crcfranc@ufpr.br (C.R.C.F.); edneaama@ufpr.br (E.A.d.S.R.)
- ² Internal Medicine Department, Division of Nephrology, Universidade Federal do Paraná, Curitiba 80060-900, Brazil; fellype.barreto@ufpr.br
- * Correspondence: andreastinghen@ufpr.br

Abstract: Podocyte dysfunction plays a crucial role in renal injury and is identified as a key contributor to proteinuria in Fabry disease (FD), primarily impacting glomerular filtration function (GFF). The $\alpha 3\beta 1$ integrins are important for podocyte adhesion to the glomerular basement membrane, and disturbances in these integrins can lead to podocyte injury. Therefore, this study aimed to assess the effects of chloroquine (CQ) on podocytes, as this drug can be used to obtain an in vitro condition analogous to the FD. Murine podocytes were employed in our experiments. The results revealed a dose-dependent reduction in cell viability. CQ at a sub-lethal concentration (1.0 $\mu\text{g}/\text{mL}$) induced lysosomal accumulation significantly ($p < 0.0001$). Morphological changes were evident through scanning electron microscopy and immunofluorescence, highlighting alterations in F-actin and nucleus morphology. No significant changes were observed in the gene expression of $\alpha 3\beta 1$ integrins via RT-qPCR. Protein expression of $\alpha 3$ integrin was evaluated with Western Blotting and immunofluorescence, demonstrating its lower detection in podocytes exposed to CQ. Our findings propose a novel in vitro model for exploring secondary Fabry nephropathy, indicating a modulation of $\alpha 3\beta 1$ integrin and morphological alterations in podocytes under the influence of CQ.

Keywords: chloroquine; Fabry disease; podocyte injury

Key Contribution: Podocyte injury is indicative of Fabry nephropathy. The deregulation of $\alpha 3\beta 1$ integrin, the primary podocyte's adhesion molecule in podocytes, could exacerbate podocyturia, contributing to the loss of kidney function. Chloroquine has been demonstrated as an in vitro model for Fabry disease, inducing significant morphological changes in podocytes that may ultimately lead to podocyte detachment.



Citation: Bosquetti, B.; Santana, A.A.; Gregório, P.C.; Cunha, R.S.d.; Miniskosky, G.; Budag, J.; Franco, C.R.C.; Ramos, E.A.d.S.; Barreto, F.C.; Stinghen, A.E.M. The Role of $\alpha 3\beta 1$ Integrin Modulation on Fabry Disease Podocyte Injury and Kidney Impairment. *Toxins* **2023**, *15*, 700. <https://doi.org/10.3390/toxins15120700>

Received: 6 October 2023

Revised: 25 November 2023

Accepted: 12 December 2023

Published: 14 December 2023



Copyright: © 2023 by the authors. Licensee MDPI, Basel, Switzerland. This article is an open access article distributed under the terms and conditions of the Creative Commons Attribution (CC BY) license (<https://creativecommons.org/licenses/by/4.0/>).

1. Introduction

Fabry disease (FD) is a rare, hereditary, X-linked pathology caused by various mutations in the *GLA* gene, responsible for encoding the α -galactosidase A (α -GLA) enzyme [1,2]. The lack of this enzyme or its low activity results in the lysosomal accumulation of glycosphingolipids, notably globotriaocilceramide (Gb3) [3,4]. Progressive Gb3 deposition in lysosomes affects various cell types, leading to renal, cardiac, and/or cerebrovascular complications [5–8]. Renal involvement stands out as a major contributor to mortality and disability in FD. Classic manifestations include glomerular injury, glomerulosclerosis, proteinuria, and microalbuminuria, ultimately progressing to end-stage renal disease [6]. Podocytes, essential for the glomerular filtration process and having a structural role, are significantly affected by FD. Podocytary dysfunction or injury is a common consequence

of various glomerulopathies and is linked to the gradual, asymptomatic decline in renal function [9,10].

FD closely mirrors the effects induced by chloroquine (CQ) or hydroxychloroquine (HCQ). These effects encompass signs, symptoms, and cellular changes observed in patients on chronic use of CQ or HCQ, including cardiomyopathy, proteinuria, and lysosomal inclusions in renal and cardiac tissues [11–15]. The amphiphilic nature of these molecules is responsible for these side effects, leading to their accumulation in lysosomes. This accumulation elevates lysosomal pH, alters the organelle's membrane permeability, and causes enzymatic dysfunction [11,16,17]. Consequently, CQ and HCQ could potentially induce a phenocopy of FD, although their specific impact on podocytes remains unclear.

The pathophysiological mechanisms leading to podocyte dysfunction in the Glomerular Basal Membrane (GBM) remain unclear. It is established that the primary mediator of the binding between the actin cytoskeleton and GBM components is the $\alpha3\beta1$ integrin [18]. In the present study, we aimed to assess the cellular and molecular mechanisms and effects of CQ on podocyte injury in vitro. Podocyte alterations have the potential to reduce adhesion to the GBM, a characteristic of podocyturia and proteinuria conditions in FD patients. Progress in this field may contribute to the development of new therapeutic interventions to enhance patient survival.

2. Results

2.1. CQ Decreases Podocyte Viability

To determine the appropriate CQ concentration, a dose–response curve experiment was performed to evaluate cell viability in endothelial cells across different CQ concentrations (1.0, 2.0, 3.0, 4.0, and 5.0 $\mu\text{g}/\text{mL}$). CQ significantly decreased cell viability ($p < 0.0001$) at concentrations of 2.0, 3.0, 4.0, and 5.0 $\mu\text{g}/\text{mL}$ (Figure 1). Notably, a concentration of 1.0 $\mu\text{g}/\text{mL}$ CQ did not impact cell viability, and this concentration was chosen for subsequent experiments.

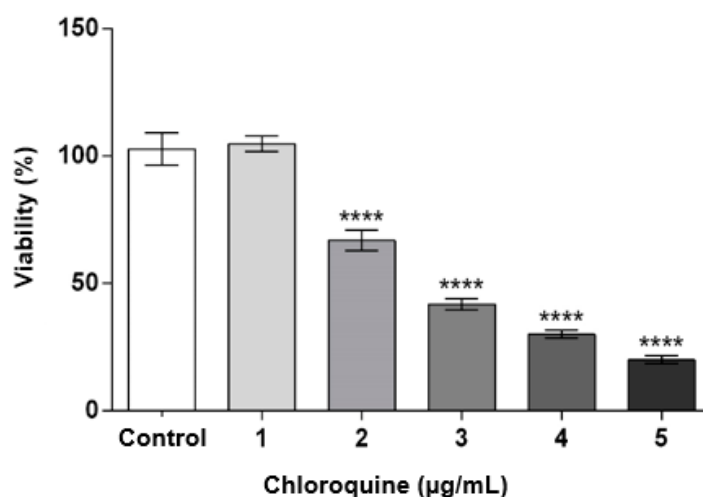


Figure 1. Dose–response curve of podocyte cells at different concentrations of CQ. Data were expressed as mean \pm SEM of four independent experiments. The results were analyzed using ANOVA ($p > 0.0001$) and Dunnett's multiple comparison test, in which **** $p < 0.0001$: 2 $\mu\text{g}/\text{mL}$ vs. control + 3 $\mu\text{g}/\text{mL}$ vs. control + 4 $\mu\text{g}/\text{mL}$ vs. control + 5 $\mu\text{g}/\text{mL}$ vs. control.

2.2. CQ Promotes Acid Organelle Accumulation

Once a non-lethal concentration of CQ was determined for the treatment of podocytes, the experiments were performed to demonstrate the increase in acid organelle accumulation (Figure 2) and the increase in lysosomal inclusions (Figure 3). A significant increase ($p < 0.0001$) in the amount and/or size of acidic organelles was observed at a concentration of 1.0 $\mu\text{g}/\text{mL}$ (Figure 2). Figure 3 shows the markings for the lysosomes in red and

the markings for the nucleus in blue. In Figure 3A,B, the lysosomal marking reflects the normal cellular constitution, with the lysosomes dispersed evenly in the cell cytoplasm. In Figure 3C,D, cell labeling becomes much more pronounced, demonstrating that there is a large increase in the number of lysosomes. These results confirm the lysosomal accumulation induced by CQ. Additionally, cells treated with CQ exhibited a more elongated appearance, fewer cell-to-cell interactions, and morphological changes in the nucleus. To further assess this, an ultrastructural analysis of the cells was performed.

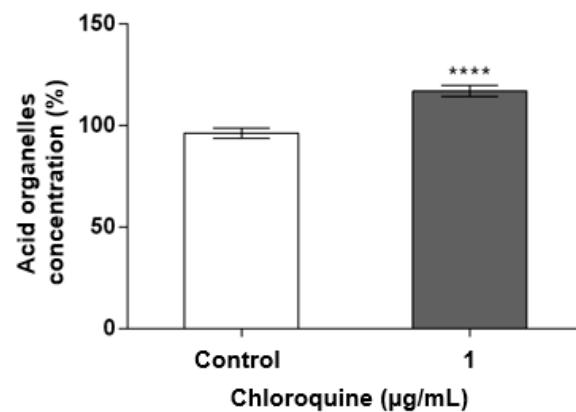


Figure 2. CQ induces increase in acid organelles. Podocytes were incubated with 1.0 µg/mL of CQ or vehicle control (culture medium) for 72 h. Acid organelles were assessed using NR and VC methods. Result is expressed as % of control (vehicle) and represents the mean ± SEM of three independent experiments. The results were analyzed using *t* test. **** $p < 0.0001$.

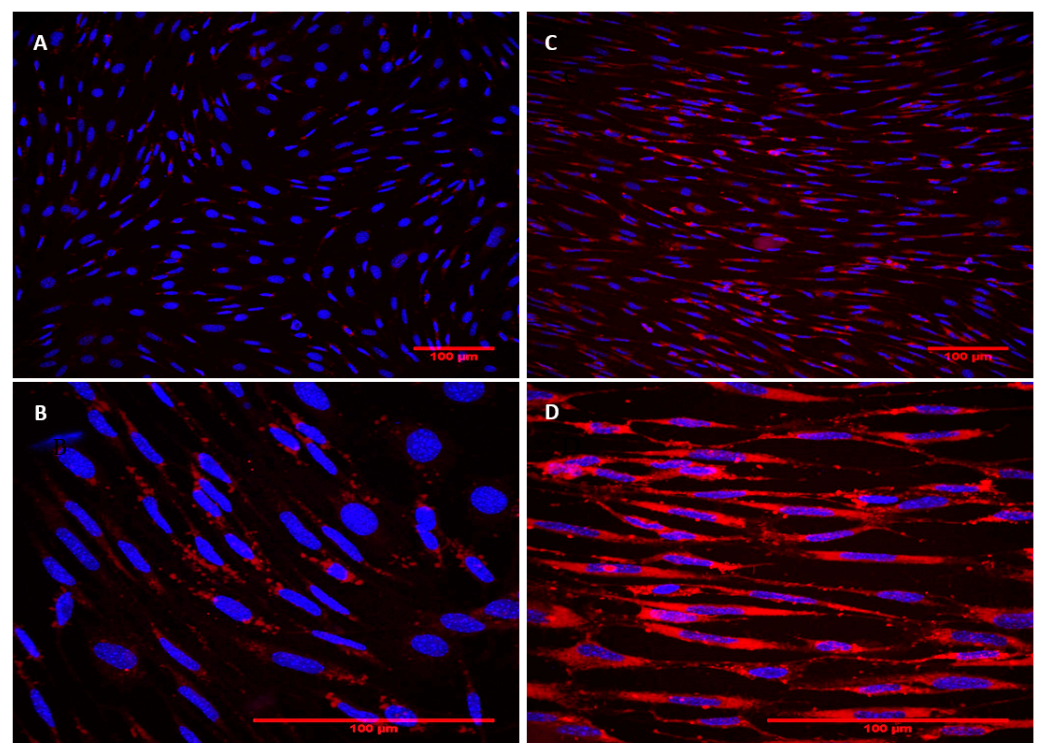


Figure 3. CQ induces increase in lysosomal inclusions. Podocytes were treated with CQ (1 µg/mL) or vehicle control (culture medium) for 72 h at 37 °C. The lysosomes (red) and nucleus (blue) were marked with the probes LysoTracker® DND-99 and DAPI, respectively. (A) Control cells (treated with culture medium)—200× magnification; (B) control cells (treated with culture medium)—600× magnification; (C) treated cells—200× magnification; and (D) treated cells—600× magnification.

2.3. CQ Promotes Podocyte Structural Changes

In order to observe morphological and ultrastructural changes in podocytes induced via lysosomal accumulation, SEM was performed (Figure 4).

Figure 4A–F depict control cells (cultured media alone). In Figure 4A,B, these cells exhibit an organized arrangement without overlap, indicating inhibited contact. They adhere well to the substrate, presenting an elongated, spindle-shaped morphology with consistent membrane projections. Figure 4A,B also show some cell debris, likely a result of prolonged culture, suggesting potential cell death or membrane debris. Figure 4C provides a closer view of characteristic membrane projections known as filopodia. In Figure 4C–E, microspheres are evident on the cell surface, with close contact and adhesion to the substrate.

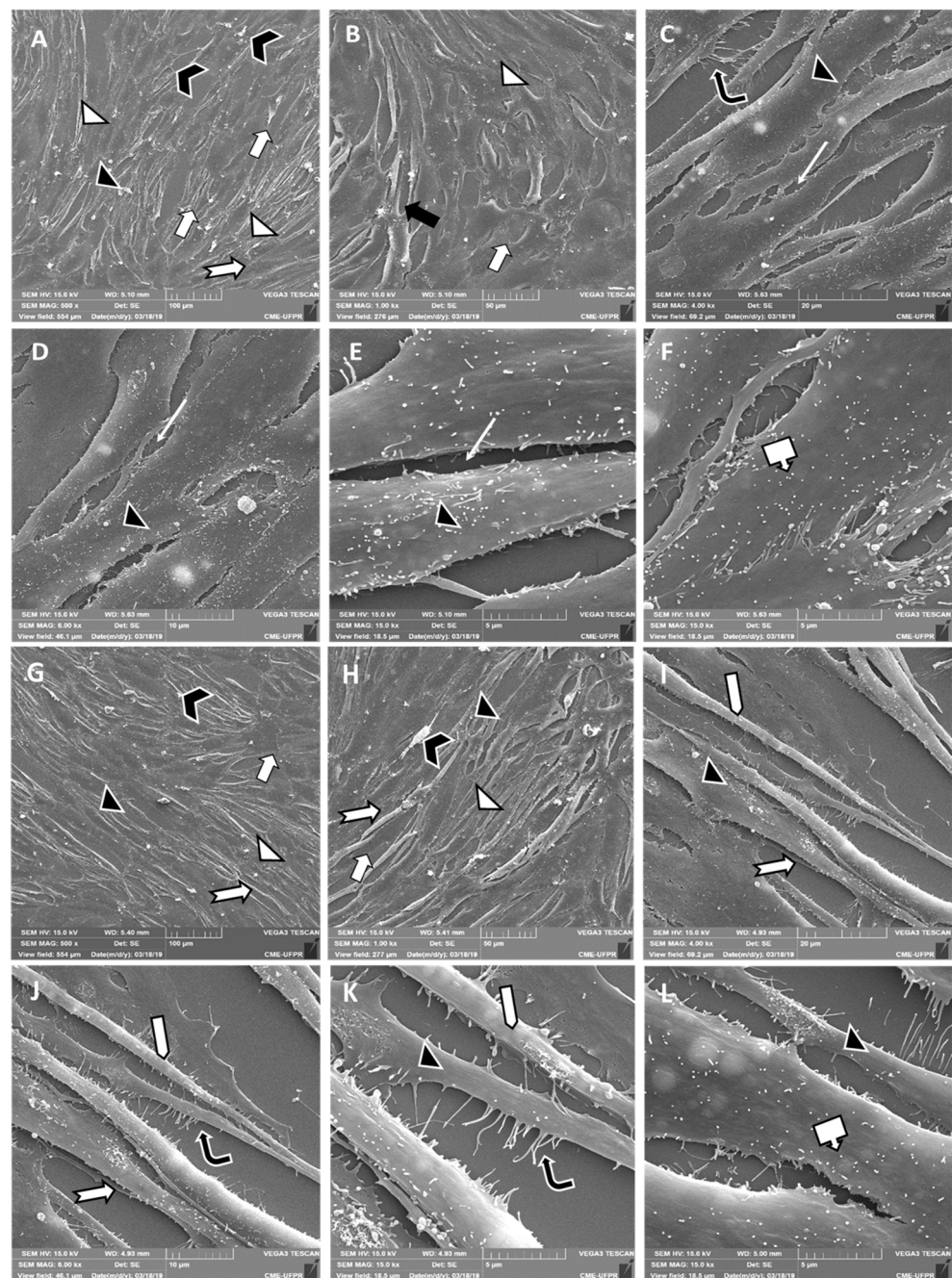


Figure 4. Cont.

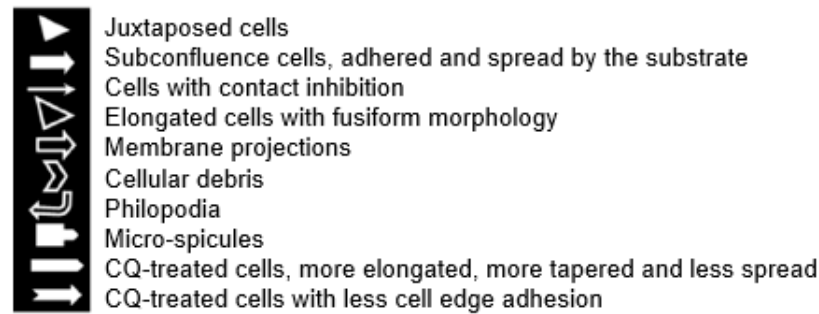
Legend:

Figure 4. Ultrastructural differences between control cells and CQ-treated cells via SEM. Images (A–F) represent control cells maintained in cell culture for 17 days only in the presence of fetal bovine serum and medium (14-day maintenance period to induce cell differentiation). The (G–L) images show cells maintained in culture for 14 days only in the presence of medium and fetal bovine serum for cell differentiation, later exposed to CQ (1 $\mu\text{g}/\text{mL}$) for a 72 h period. Images (A,G) are enlarged at 500 \times , (B,H) at 1000 \times , (C,I) at 4000 \times , (D,J) at 6000 \times , and (E,F,K,L) at 15,000 \times .

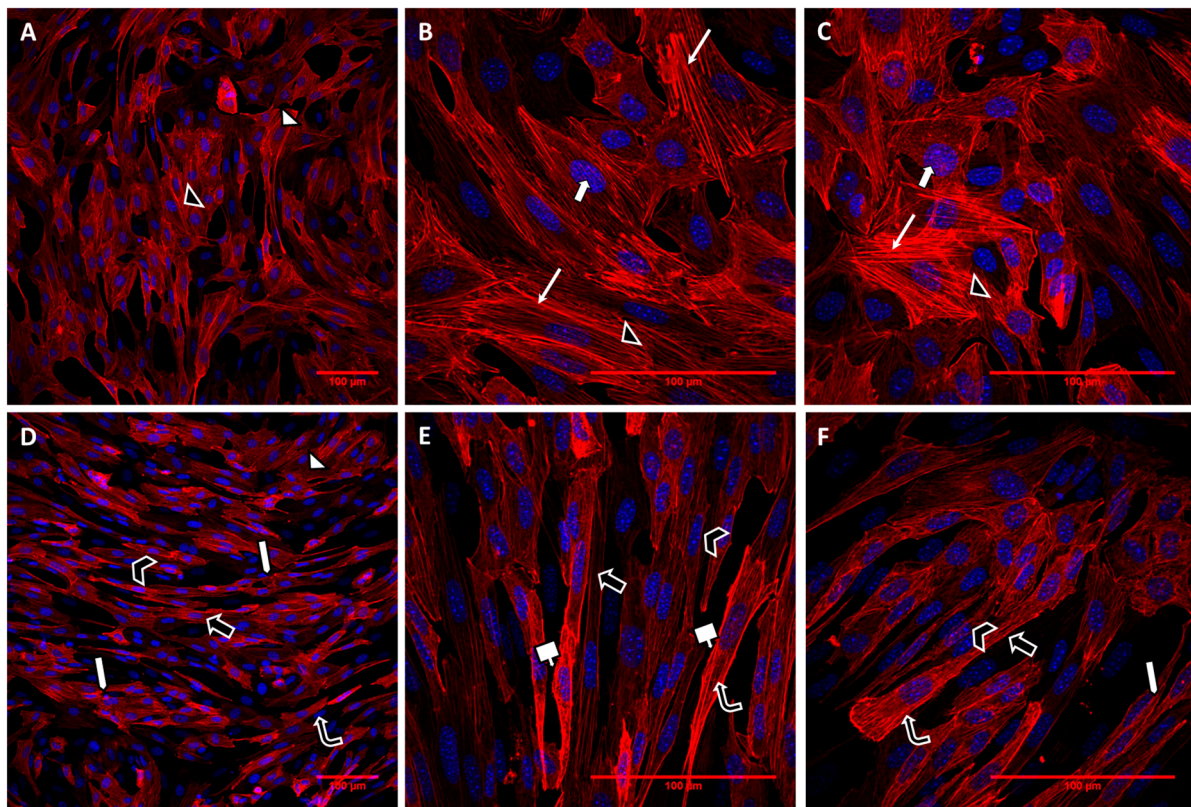
Figure 4G–L show the cells exposed to CQ. In Figure 4G,H, the cells have morphological patterns and culture organization similar to those observed for the control cells. Notably, CQ-treated cells are adherent and spread out, with an elongated morphology and a fusiform pattern. Additionally, these cells are not stacked on top of each other, demonstrating contact inhibition. Cell debris is also observed throughout the cell culture. In Figure 4I,J, it is evident that the cell bodies are losing adhesion to the substrate, with cells appearing less spread out and less adhered. Figure 4J,K also show cells with less lateral expansion of the cell body and an elongated, tapered, and narrow morphology.

In summary, the treatment with CQ via ultrastructural analysis shows cells with a loss of adhesion and a lower degree of spreading and lateral expansion of the cell body when compared to control cells.

In order to evaluate the F-actin cytoskeleton after treatment of cells with CQ, the staining was performed with the ActinRedTM 555 Rhodamine phalloidin probe, as can be seen in Figure 5.

Figure 5A–C display images of control cells, while Figure 5D–F depict cells treated with CQ, as described previously. In Figure 5A–C, control cells exhibit intense marking and organized actin microfilaments. The nuclei of these cells are spherical and centrally located within the cell body, showcasing a clear organization of stress fibers throughout. These cells, elongated and spindle-shaped, demonstrate adherence and substantial interaction with the substrate. They are either juxtaposed or sub-confluent. Interestingly, Figure 5D–F reveal a noticeable change in the lateral spreading of cell bodies after exposure to CQ. The nuclei remain centrally located but undergo morphological changes, becoming visibly elongated and following the cell's overall shape. The cells appear significantly more elongated and spindle-shaped, displaying intense markings of predominantly deposited actin microfilaments. Notably, the submembrane cortex shows a less intense organization of microfilaments in stress fibers throughout the cell body. Actin microfilaments are now present in reduced form in long filaments due to the extension of the cell body. In this context, the cells lose their ability to organize stress fibers for lateral expansion, resulting in reduced spreading and lateral adhesion to the substrate.

The CQ treatment in the podocytes evidently induced loss of adhesion, a lower degree of spreading, and decreased organization of stress fibers, inducing more elongated, fusiform cells with less expansion of the cell body.



Legend:










	Actin microfilaments
	Predominance of central and spherical nucleus
	Stress fibers throughout the cell body
	Adhered cells, spread, showing lateral extension of the cell body, intimate substrate interaction
	CQ-treated cells showing decreased lateral spreading of the cell body
	Predominance of central, stretched and fusiform nucleus
	CQ-treated cells with stretched and fusiform morphology
	Predominance of actin microfilaments in the submembrane cortex
	Reduction of the organization of actin microfilaments in stress fibers

Figure 5. Fluorescence analysis of CQ-treated cells under confocal microscopy. Images (A–C) represent control cells maintained in cell culture for 17 days only in the presence of fetal bovine serum and medium (14-day maintenance period to induce cell differentiation). Images (D–F) show cells maintained in culture for 14 days only in the presence of medium and fetal bovine serum for cell differentiation. Subsequently, they were exposed to QC (1 $\mu\text{g}/\text{mL}$) for a period of 72 h. Images (A,D) are 200 \times magnified, and images (B,C,E,F) are 600 \times magnified.

2.4. Effects of CQ on $\alpha 3\beta 1$ Integrin

The gene expression of the $\alpha 3$ and $\beta 1$ integrin chains was evaluated using RT-qPCR in podocytes treated or not with CQ (1 $\mu\text{g}/\text{mL}$) at 37 $^{\circ}\text{C}$ for 72 h. The evaluated genes were *Itgb1* and *Itga3*, representing each of the $\alpha 3\beta 1$ integrin chains, respectively. Our data showed no statistical difference between treatment groups for both integrin genes (Figure S1). Also, the protein expression of the $\alpha 3$ integrin chains was evaluated via Western Blotting, in which no statistical difference was observed between podocytes treated or not with CQ (Figure 6).

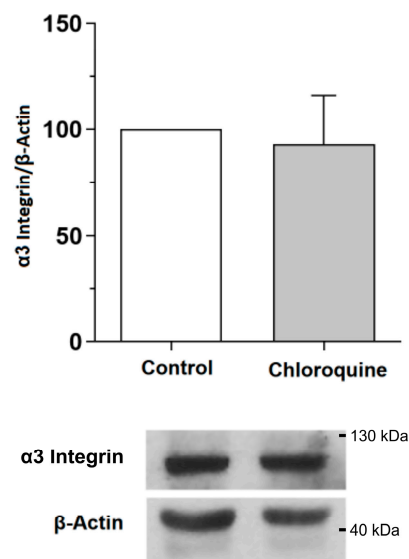


Figure 6. Quantitative analysis of $\alpha 3$ integrin via Western Blotting. Analysis of $\alpha 3$ integrin protein extracts in untreated (control) or CQ-treated ($1 \mu\text{g}/\text{mL}$) podocytes for 72 h at 37°C . The values refer to the mean \pm SEM of three independent experiments ($n = 3$). The data were analyzed using the Mann–Whitney test ($ns > 0.05$).

In order to evaluate the cellular distribution of $\alpha 3$ integrin after treatment of cells with CQ, an immunofluorescence assay was performed. Figure 7A,B depict control cells, while Figure 7C,D display images of cells treated with CQ, as described previously. In Figure 7A, spherical nuclei and actin microfilaments are observed. However, elongated cells with fusiform nuclei and actin microfilaments in stress fibers are observed after exposure to CQ (Figure 7C). Notably, Figure 7B–D reveal the detection of clustered $\alpha 3$ integrin, with reduced labeling in cells that received treatment with CQ (Figure 7D).

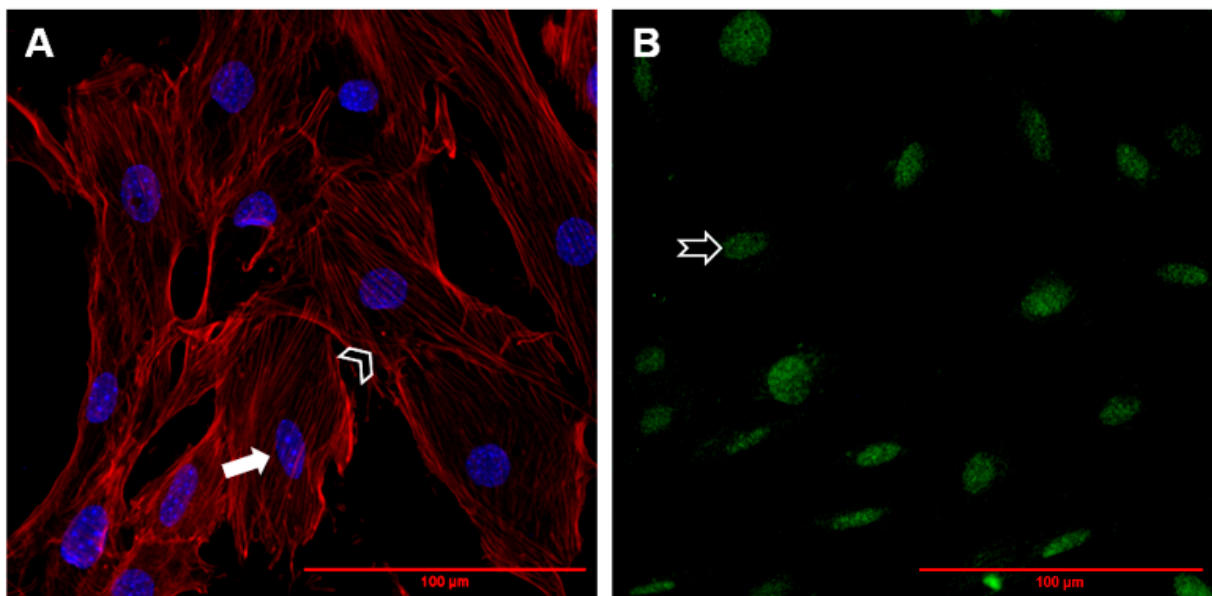


Figure 7. Cont.

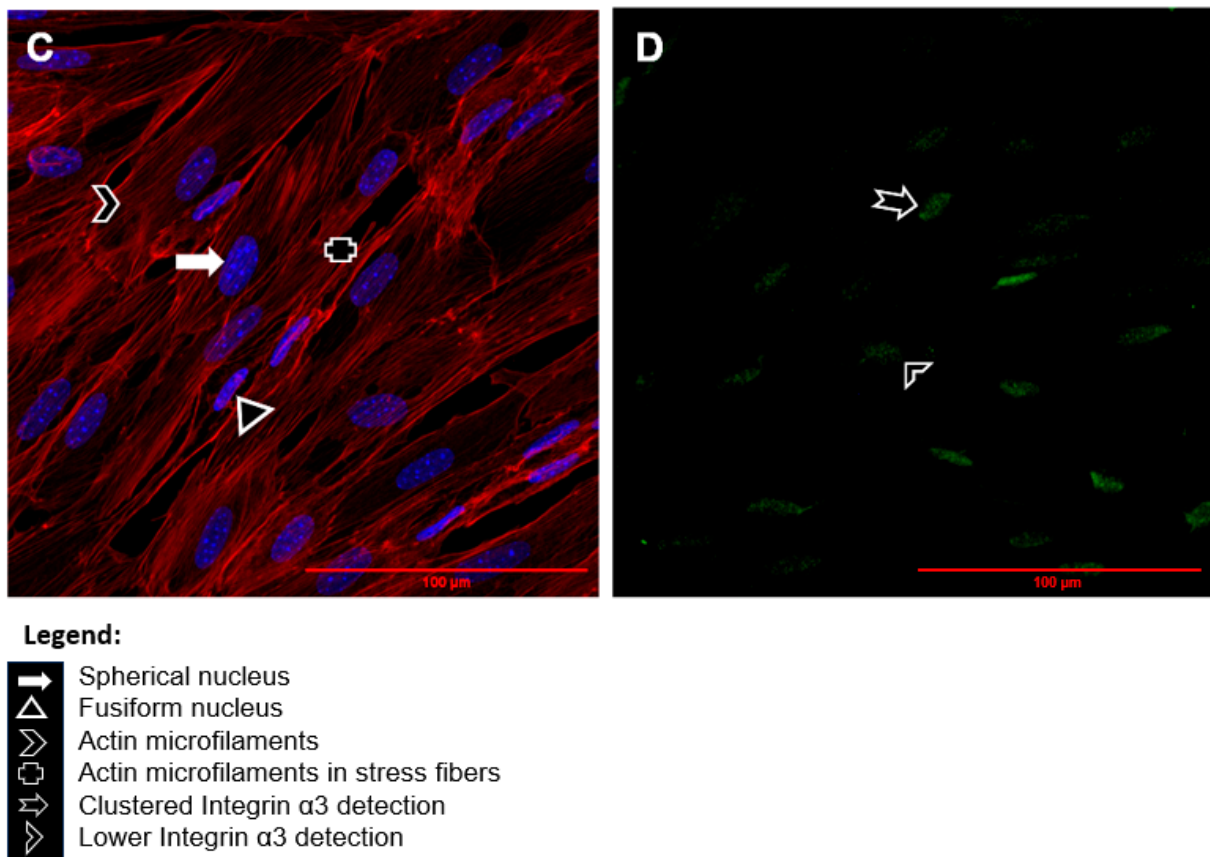


Figure 7. Fluorescence analysis of $\alpha 3$ integrin under confocal microscopy. Images (A,B) represent control cells. Images (C,D) represent cells exposed to QC (1 $\mu\text{g}/\text{mL}$) for a period of 72 h. The (B,D) images show clustered $\alpha 3$ integrin with lower detection after exposition to CQ. The nucleus (blue) was marked with DAPI, the F-actin cytoskeleton (red) was marked with the ActinRed™ 555 Rhodamine phalloidin probe, and $\alpha 3$ integrin (green) was marked with the Alexa Fluor® 647 Phalloidin probe, respectively. All images are 600 \times magnified.

3. Discussion

Podocytes are highly specialized epithelial cells that cover the glomerular basement membrane (GBM) through their cell extensions called pedicels [19]. These cells are a very important component in the glomerular filtration barrier (GFB), as they are involved in the synthesis of GBM and interact with the endothelium to maintain its viability, thus forming a structure in which the blood filtration process occurs [20].

The present study shows that the CQ can reduce the cell's viability in a dose-dependent manner (Figure 1) and, at a sub-lethal concentration (1.0 $\mu\text{g}/\text{mL}$), promotes lysosomal accumulation (Figures 2 and 3). This result corroborates what has already been described for patients who make chronic use of this medication and develop signs and symptoms of kidney impairment, as occurs in FD [11]. As a result of this cellular dysfunction, podocytes treated with CQ showed changes in cell morphology, as shown in Figures 4 and 5. Podocyte morphology, including its cell extensions, is all sustained based on the actin-F cytoskeleton, and its structure is essential for these cells to play their role in GFB.

Utilizing immortalized endothelial cells, Inagaki et al. demonstrated that CQ's specific reduction in α -GAL activity resulted in ultrastructural changes such as the formation of lysosomal inclusions of glycosphingolipids [21]. More recently, we demonstrated the same phenomenon in endothelial cells, albeit at half the CQ concentration used in the prior study [22]. CQ is acknowledged for altering lysosomal properties, including increased pH and changes in membrane permeability and enzyme activity [11,16,17]. Cellular lipid accumulation is recognized to initiate a cascade of proinflammatory and profibrotic pathways

in FD, leading to cellular structural changes, tissue damage, and ultimately, organ dysfunction [23]. Renal impairment stands out as a primary contributor to death and disability in FD, and podocyte dysfunction is one of the main causes of Fabry nephropathy [6,19,24].

Due to cellular dysfunction, podocytes treated with CQ exhibited alterations in both morphology and structure. Our findings align with Kang et al.'s (2020) study, reporting disruption of the actin cytoskeleton and reduced motility in human podocytes treated with 25 μ M of CQ for 24 and 48 h [25]. This study also identified differential expression of lysosome-related proteins and cell adhesion molecules in CQ-exposed podocytes, potentially influencing cell stability [25]. The maintenance of podocyte morphology, including cell extensions, relies on the F-actin cytoskeleton, a structure crucial for the proper functioning of the glomerular filtration barrier (GFB). Previous studies have demonstrated that mutations in genes encoding proteins responsible for linking the F-actin cytoskeleton with focal adhesion proteins can result in podocyte damage, the thinning of pedicels, proteinuria, and the development of a glomerular disorder [19,26,27]. Given the significance of podocyte morphology, alterations in the F-actin cytoskeleton may have serious implications for the functions of these cells.

The α 3 β 1 integrin is the major protein that links the actin-F cytoskeleton with the GBM and, consequently, is the most important protein that regulates the podocyte's focal adhesion [18,28]. We focused on assessing the expression of α 3 integrin, which is known to have a significant effect on podocyte adhesion [18,28]. Our data did not indicate significant changes in gene expression and protein levels in podocytes in the presence of CQ with RT-qPCR and Western Blotting; although there was less detection of α 3 integrin in immunofluorescence, as can be seen in Figure 7. The protein reduction in α 3 integrin demonstrated in the exposed results reinforces its direct relationship with the structural abnormality of podocytes, a fact that may contribute to nephropathy in patients with FD. These results demonstrate that CQ presents toxicity for these cells and, consequently, can impair kidney function. However, protein levels and the cellular distribution of β 1 integrin remain yet to be analyzed. The dysregulation in the gene expression of these two chains also occurs in patients with diabetic nephropathy (DN), who present the following symptoms: podocyte detachment of the GBM, erasure of the pedicels in renal biopsy, podocyturia, microalbuminuria, and proteinuria [29–32]. In vivo studies showed that disorders targeting α 3 integrin, such as mutation and deletion, can, respectively, prevent the formation of pedicels in podocytes, compromising glomerular development and causing glomerular injury in mice [33,34]. Also, Chen et al. have demonstrated that there is an in vitro decrease in the protein expression of α 3 β 1 integrin as well as a decrease in the capacity of podocyte adhesion in DN [35]. Therefore, the α 3 β 1 integrin deregulation may be related to glomerulopathies such as the congenital nephrotic syndrome [36,37].

We recognize that the present study has some limitations. The podocyte model used for the tests was murine because of the difficulty in obtaining human podocytes. In addition, we evaluated the α 3 β 1 gene expression and only the protein expression of the α 3 subunit. Evaluation of β 1 subunit expression would be the next step to investigate the involvement of deregulation of this heterodimer in this pathway. This is expected to provide valuable insights into the mechanism that leads to the GBM detachment of podocytes in FD.

4. Conclusions

The main findings of the present study reveal that treatment with CQ at sub-lethal doses (1.0 μ g/mL) can induce alterations in podocytes, including lysosomal lipid accumulation (mimicking FD), cytoskeletal remodeling, and morphological and structural changes. In essence, we propose a podocyte model for the study of FD. Moreover, the expression profile of the primary focal podocyte adhesion integrin in response to lysosomal accumulation was demonstrated. The same profile is observed in DN and in vivo data, also indicating a parallel progression of these two diseases. Consequently, the results obtained present potential avenues for new therapeutic targets aimed at enhancing the quality of life for these patients.

5. Materials and Methods

5.1. Reagents

RPMI 1640 medium (RPMI), fetal bovine serum (FBS), collagen I from rat tail, and Penicillin/Streptomycin were purchased from Gibco (Grand Island, NE, USA). Fluoromount G and DAPI were obtained from Life Technologies (Carlsbad, CA, USA). LysoTracker[®] DND-99 probe, Alexa Fluor[®] 647 Phalloidin, and Actin Red[™]555 ReadyProbes[™] Rhodamine phalloidin were commercially obtained (Thermo Scientific, Waltham, MA, USA). Murine Interferon Gamma (IFN- γ) was purchased from Preprotech. [4, 5-dimethyl-thiazol-2-yl]-2, 5-diphenyltetrazolium bromide (MTT), neutral red solution (NR), and dimethyl sulfoxide (DMSO) were obtained from Sigma-Aldrich (St. Louis, MO, USA). CQ was purchased from Cristália (São Paulo, Brazil). Western Blotting reagents were obtained from GE HealthCare Life Sciences (Little Chalfont, UK). All other reagents were obtained from Sigma-Aldrich (St. Louis, MO, USA) if not otherwise specified.

5.2. Podocyte Cell Culture and Treatment Conditions

The immortalized murine kidney podocyte cell line E11 obtained from Cell Lines Service (Eppelheim, Germany) was kindly provided by Prof. Dr. Niels Olsen Saraiva Câmara (Federal University of São Paulo—UNIFESP). For the podocyte culture, a collagen I matrix (0.5 mg/mL) should be made on the plates. The undifferentiated cells were grown under permissive conditions in RPMI 1640 medium supplemented with 10% FBS and IFN- γ at a concentration of 20–50 IU/mL, maintained at 33 °C in a humidified atmosphere containing 5% CO₂. After reaching about 70–80% confluence, the cells were exposed to a non-permissive condition to start the cell differentiation process. In this phase, the cells were placed in an atmosphere at 37 °C and 5% CO₂, with a culture medium without INF- γ . After 14 days of cultivation, cells were ready for experiments [38,39]. In the sequence, the cells were exposed to CQ [21].

5.3. Cell Viability Assay

Cell viability was assessed using the MTT assay [40]. Podocytes were plated into 96-well culture plates at a density of 1×10^3 cells per well. After 24 h of incubation, the medium was replaced, and the cells were treated with CQ for 72 h. Then, this medium was replaced with fresh medium (100 μ L/well), and 10 μ L of MTT (Sigma-Aldrich, Hercules, CA, USA) solution (5 mg/mL in D-PBS) was added to each well. The plate was incubated for 4 h at 37 °C. Subsequently, the media was removed and replaced with DMSO to dissolve the crystals of reduced formazan, and the absorbance was then measured at 570 nm in a Bio-Rad 680 microplate reader (CA, USA). Four experiments were performed in duplicate.

5.4. Acid Organelle Accumulation Assay

Podocytes were plated into 96-well plates (1×10^3 cells/well) and treated with CQ (1 μ g/mL) or vehicle control (culture medium) for 72 h. Next, all medium was removed, and 100 μ L of NR solution (40 μ g/mL) was added. Subsequently, the plate was incubated for 3 h at 37 °C and 5% CO₂. Finally, the NR-containing medium was removed, the cells were washed with 150 μ L of PBS per well, and 150 μ L of distain solution (1% glacial acetic acid and 48% ethanol) was added. The absorbance was measured using a 540 nm filter spectrophotometer [41]. NR stains lysosomes as color is pH-dependent. After the NR assay, the solution was removed from the wells and washed once with PBS (200 μ L/well). Next, 100 μ L of violet crystal (VC) solution (0.25 mg/mL) was added per well, and the plates were incubated for 20 min at room temperature (22 °C). Then, the wells were washed 2 \times with PBS and solubilized with 33% acetic acid. Finally, the absorbance was measured using a spectrophotometer at a wavelength of 570 nm. The result was obtained by normalizing the NR test to the VC. Three experiments were performed in duplicate.

5.5. Fluorescence Lysosome Inclusions Visualization Assay

The LysoTracker[®] DND-99 fluorescent probe was used for visualization of acid organelle inclusions such as lysosomes since lysosome size is related to the number of inclusions. The cells were plated on coverslips and treated with CQ at 1.0 µg/mL. The treatment medium was removed, and cells were washed twice with sterile PBS. Next, cells were incubated for 90 min at 37 °C with 50 nM of LysoTracker[®] DND-99 probe diluted in culture medium and subsequently washed twice with PBS, fixed with 2% paraformaldehyde for 20 min, and washed again with PBS. The coverslips were mounted on histological slides with Fluoromont-G[™] with DAPI mounting medium, sealed with formaldehyde-free color enamel, and observed under a Nikon A1RSiMP confocal microscope (NIKON, Tokyo, Japan). Three experiments were performed in duplicate.

5.6. Actin-F Cytoskeleton and α3 Integrin Visualization Assay

The Alexa Fluor[®] 647 Phalloidin fluorescent probe was used for visualization of integrin α3 localization, and the ActinRed[™] 555 Rhodamine phalloidin probe was used for visualization of the actin-F cytoskeleton. The cells were plated on coverslips and treated with CQ at a 1.0 µg/mL concentration, as described before. Subsequently, the medium was removed, and the coverslips were washed twice with PBS. The cells were fixed with 2% paraformaldehyde (PFA) diluted in PBS for 20 min at room temperature (22 °C). After fixation, the cells were washed twice with PBS and incubated with integrin α3 antibody (1:1000, Thermo Fisher Scientific, Waltham, MA, USA) overnight at 4 °C. Alexa Fluor[®] 647 Phalloidin was diluted in a solution of 0.01% saponin in PBS and added for 1 h. Posteriorly, the cells were incubated with ActinRed[™] 555 Rhodamine phalloidin for 45 min. The coverslips were mounted on a histological slide containing Fluoromont g with DAPI. After this process, the coverslips were sealed with formaldehyde-free color enamel, and visualization was performed using a Nikon A1RSiMP confocal microscope (NIKON, Tokyo, Japan). Three experiments were performed in duplicate.

5.7. Integrins α3 and β1 Gene Expression

The total RNA of podocytes was isolated from cells lysed with Trizol (Invitrogen, Carlsbad, CA, USA), according to the manufacturer's recommendations. The purity and concentration of the RNA were verified with the 260/280 nm ratio measured on the NanoDrop 2000 spectrophotometer (Thermo Scientific, Waltham, MA, USA). The RNA integrity was analyzed via agarose gel electrophoresis. The mRNA molecules were converted into complementary DNA (cDNA) using the High-Capacity RNA-to-cDNA kit (Applied Biosystems, Waltham, MA, USA). For RT-qPCR, the cDNA was amplified with specific primer oligonucleotides using the SYBR[™] Green PCR Master Mix (Thermo Scientific, Waltham, MA, USA) in the StepOne Plus[™] Real Time PCR System (Thermo Scientific, Waltham, MA, USA) thermocycler. The relative expressions of the genes were analyzed using the 2^{-ΔΔCT} method. The genes analyzed were *Rplp0* (ribosomal protein lateral stalk subunit P0), *Itgb1* (Integrin Subunit Beta 1), and *Itga3* (Integrin Subunit Alpha 3). The sequences of the oligonucleotides initiating the target genes are described in Table 1. Five experiments were performed in duplicate.

Table 1. Primer oligonucleotides used in RT-qPCR.

Gene	Oligonucleotides *
<i>Itgb1</i>	5'-AACTTGTTGGTCAGCAACGC-3' (F)
	5'-AACCGCAACCTGCATGATTG-3' (R)
<i>Itga3</i>	5'-CCTCTTCGGCTACTCGGTC-3' (F)
	5'-CCGGTTGGTATAGTCATCACCC-3' (R)
<i>Rplp0</i>	5'-CGACCTGGAAGTCCAACACTAC-3' (F)
	5'-ACTTGCTGCATCTGCTTG-3' (R)

* F, forward; R, reverse.

5.8. Analysis of Integrin $\alpha 3$ Levels via Western Blotting

The cells were cultured (3×10^5 cells/dish) in 100 mm dishes and were stimulated for 72 h with CQ at a concentration of 1.0 $\mu\text{g}/\text{mL}$ for 72 h. The cells were washed with ice-cold PBS and lysed in 100 μL of radioimmunoprecipitation assay buffer (50 mM sodium chloride, 1.0% Triton X-100, 0.5% sodium deoxycholate, 0.1% SDS, 50 mM Tris, pH 8.0) for 20 min. The cell lysates were centrifuged for 20 min at $12,000 \times g$ at 4 °C, and the supernatants were collected. Equal amounts of protein (30 μg) were separated using 8% sodium dodecyl sulfate-polyacrylamide gel electrophoresis and transferred to nitrocellulose membranes (GE HealthCare Life Sciences, Little Chalfont, UK). The membranes were blocked for 1 h at room temperature with Tris-buffered saline containing 0.05% Tween 20 (TBS-T) and 3% casein. After washing with TBS-T, the membranes were incubated overnight with the integrin $\alpha 3$ antibody (1:1000, Thermo Fisher Scientific, Waltham, MA, USA) at 4 °C with gentle shaking. The primary antibodies were detected using horseradish peroxidase-conjugated goat anti-rabbit IgG and visualized using enhanced chemiluminescence Western Blotting reagents (GE HealthCare Life Sciences, Little Chalfont, UK). Band intensity was analyzed using Software Image Studio Lite 5.2 (Lincoln, NE, USA). All analyses were performed in triplicate.

5.9. Morphological and Ultrastructural Analysis Performed via a Scan Electronic Microscopy

The SEM was the technique used for the evaluation of possible morphological changes and was ultra-adapted through the accumulation of lysosomes in the podocytes. The cells were plated (1×10^5 cells/coverslips) in circular coverslips (13 mm in diameter) at a 24-well plate and were treated with CQ at a concentration of 1.0 $\mu\text{g}/\text{mL}$ for 72 h. After treatment, the medium was removed, and the cells were washed twice with PBS and fixed with Karnovskí's solution (2% glutaraldehyde, 4% paraformaldehyde, 0.1 M of CaCl_2 , and pH 7.4) for 1 h. Subsequently, they were washed with 0.1 M of sodium cacodylate buffer (pH 7.4) and post-fixed with 1% osmium tetroxide (diluted in 0.1 M of sodium cacodylate buffer, pH 7.4) for 1 h. After the fixation, the cells were washed in 0.1 M of sodium cacodylate buffer and dehydrated by increasing ethanol engines (30%, 50%, 70%, 90%, and twice with 100%) for a period of 10 min at each concentration. Next, the cells were subjected to the critical point in the CPD 010 device (Critical Point Dryer, Bal-Tec AG, Balzers, Liechtenstein) 030-Balzers, metalized with gold in the device (SCD 030-Balzers, Balzers Union, Balzers, Liechtenstein), and analyzed using a scanning electron microscope (Tescan-Vega3-LMU-Scanning electron microscope, Kohoutovice, Czech Republic) at the Center for Electronic Microscopy of Federal University of Paraná (UFPR). The images were captured in increments of $500\times$, $1000\times$, $4000\times$, $6000\times$, and $15,000\times$. Four experiments were performed in duplicate.

5.10. Data Analyses

Statistical analyses were performed using the statistical package JMP (version 8.0; SAS Institute Inc., Cary, NC, USA). Comparisons between groups were performed using a Student's *t*-test or an analysis of variance (ANOVA) with Dunnett's multiple comparison test for paired data and Mann–Whitney for unpaired data. Values were expressed as the mean \pm standard error of the mean (SEM). Three to five independent experiments were performed. $p < 0.05$ was considered statistically significant.

Supplementary Materials: The following supporting information can be downloaded at <https://www.mdpi.com/article/10.3390/toxins15120700/s1>, Figure S1: Relative expression of the *Itga3* and *Itgb1* via RT-qPCR. Increased relative expression of the *Itga3* and *Itgb1* genes in untreated (control) or CQ-treated (1 $\mu\text{g}/\text{mL}$) podocytes for 72 h at 37 °C. The relative expression of mRNA was determined with the $2^{-\Delta\Delta\text{Ct}}$ method, using *Rplp0* as a normalizing gene. The values refer to the mean \pm SEM of three independent experiments ($n = 3$). The data were analyzed using the Mann–Whitney test ($ns > 0.05$).

Author Contributions: Conceptualization, B.B., A.A.S., P.C.G., R.S.d.C., J.B., G.M. and F.C.B.; methodology, B.B., A.A.S., P.C.G., R.S.d.C., J.B. and G.M.; software, B.B. and A.A.S.; validation, B.B., A.A.S., P.C.G., R.S.d.C., J.B., G.M., C.R.C.F. and E.A.d.S.R.; formal analysis, B.B., A.A.S., P.C.G., R.S.d.C., J.B. and G.M.; investigation, B.B. and A.A.S.; resources, B.B. and A.A.S.; data curation, B.B. and A.A.S.; writing—original draft preparation, B.B. and A.A.S.; writing—review and editing and supervision, A.E.M.S. All authors have read and agreed to the published version of the manuscript.

Funding: The authors acknowledge the support from the Coordenação de Aperfeiçoamento de Pessoal de Nível Superior—Brazil (CAPES)—Finance Code 001, Conselho Nacional de Desenvolvimento Científico e Tecnológico (CNPq), and Universidade Federal do Paraná/Tesouro Nacional.

Institutional Review Board Statement: Not applicable.

Informed Consent Statement: Not applicable.

Data Availability Statement: The data presented in this study are available on request from the corresponding author.

Conflicts of Interest: The authors declare no conflict of interest.

References

- Battaglia, Y.; Fiorini, F.; Azzini, C.; Esposito, P.; De Vito, A.; Granata, A.; Storari, A.; Mignani, R. Deficiency in the Screening Process of Fabry Disease: Analysis of Chronic Kidney Patients Not on Dialysis. *Front Med. (Lausanne)* **2021**, *8*, 640876. [[CrossRef](#)] [[PubMed](#)]
- Castelli, V.; Stamerra, C.A.; d'Angelo, M.; Cimini, A.; Ferri, C. Current and Experimental Therapeutics for Fabry Disease. *Clin. Genet.* **2021**, *100*, 239–247. [[CrossRef](#)] [[PubMed](#)]
- Bichet, D.G.; Aerts, J.M.; Auray-Blais, C.; Maruyama, H.; Mehta, A.B.; Skuban, N.; Krusinska, E.; Schiffmann, R. Assessment of Plasma Lyso-Gb3 for Clinical Monitoring of Treatment Response in Migalastat-Treated Patients with Fabry Disease. *Genet. Med.* **2021**, *23*, 192–201. [[CrossRef](#)] [[PubMed](#)]
- Kok, K.; Zwiers, K.C.; Boot, R.G.; Overkleeft, H.S.; Aerts, J.M.F.G.; Artola, M. Fabry Disease: Molecular Basis, Pathophysiology, Diagnostics and Potential Therapeutic Directions. *Biomolecules* **2021**, *11*, 271. [[CrossRef](#)] [[PubMed](#)]
- Boggio, P.; Luna, P.C.; Abad, M.E.; Larralde, M. Doença de Fabry. *An. Bras. Dermatol.* **2009**, *84*, 367–376. [[CrossRef](#)]
- Nagamatsu, K.; Sekijima, Y.; Nakamura, K.; Nakamura, K.; Hattori, K.; Ota, M.; Shimizu, Y.; Endo, F.; Ikeda, S.I. Prevalence of Fabry Disease and GLA c.196G>C Variant in Japanese Stroke Patients. *J. Hum. Genet.* **2017**, *62*, 665–670. [[CrossRef](#)]
- Nakao, S.; Kodama, C.; Takenaka, T.; Tanaka, A.; Yasumoto, Y.; Yoshida, A.; Kanzaki, T.; Enriquez, A.L.D.; Eng, C.M.; Tanaka, H.; et al. Fabry Disease: Detection of Undiagnosed Hemodialysis Patients and Identification of a “Renal Variant” Phenotype. *Kidney Int.* **2003**, *64*, 801–807. [[CrossRef](#)]
- Shu, L.; Vivekanandan-Giri, A.; Pennathur, S.; Smid, B.E.; Aerts, J.M.F.G.; Hollak, C.E.M.; Shayman, J.A. Establishing 3-Nitrotyrosine as a Biomarker for the Vasculopathy of Fabry Disease. *Kidney Int.* **2014**, *86*, 58–66. [[CrossRef](#)]
- Abou Daher, A.; El Jalkh, T.; Eid, A.A.; Fornoni, A.; Marples, B.; Zeidan, Y.H. Translational Aspects of Sphingolipid Metabolism in Renal Disorders. *Int. J. Mol. Sci.* **2017**, *18*, 2528. [[CrossRef](#)]
- Liebau, M.C.; Braun, F.; Höpker, K.; Weitbrecht, C.; Bartels, V.; Müller, R.U.; Brodessa, S.; Saleem, M.A.; Benzing, T.; Schermer, B.; et al. Dysregulated Autophagy Contributes to Podocyte Damage in Fabry’s Disease. *PLoS ONE* **2013**, *8*, e63506. [[CrossRef](#)]
- Albay, D.; Adler, S.G.; Philipose, J.; Calescibetta, C.C.; Romansky, S.G.; Cohen, A.H. Chloroquine-Induced Lipidosis Mimicking Fabry Disease. *Modern Pathol.* **2005**, *18*, 733–738. [[CrossRef](#)] [[PubMed](#)]
- Costa, R.M.; Martul, E.V.; Reboledo, J.M.; Cigarrán, S. Curvilinear Bodies in Hydroxychloroquine-Induced Renal Phospholipidosis Resembling Fabry Disease. *Clin. Kidney J.* **2013**, *6*, 533–536. [[CrossRef](#)] [[PubMed](#)]
- Linthorst, G.E.; Hollak, C.E.M.; Müller-Höcker, J. Chloroquine-Induced Phospholipidosis of the Kidney Mimicking Fabry’s Disease (multiple letters). *Hum. Pathol.* **2003**, *34*, 1358–1359. [[CrossRef](#)]
- Manabe, S.; Mochizuki, T.; Sato, M.; Kataoka, H.; Taneda, S.; Honda, K.; Uchida, K.; Nitta, K. Lupus Nephritis and Hydroxychloroquine-Associated Zebra Bodies: Not Just in Fabry Disease. *Kidney Med.* **2021**, *3*, 442–446. [[CrossRef](#)] [[PubMed](#)]
- Yogasundaram, H.; Hung, W.; Paterson, I.D.; Sergi, C.; Oudit, G.Y. Chloroquine-induced cardiomyopathy: A reversible cause of heart failure. *ESC Heart Failure* **2018**, *5*, 372–375. [[CrossRef](#)] [[PubMed](#)]
- Ducharme, J.; Farinotti, R. Clinical Pharmacokinetics and Metabolism of Chloroquine. Focus on Recent Advancements. *Clin. Pharmacokinet.* **1996**, *31*, 257–274. [[CrossRef](#)]
- Gonzalez-Noriega, A.; Grubb, J.H.; Talkad, V.; Sly, W.S. Chloroquine Inhibits Lysosomal Enzyme Pinocytosis and Enhances Lysosomal Enzyme Secretion by Impairing Receptor Recycling. *J. Cell Biol.* **1980**, *85*, 839–852. [[CrossRef](#)]
- Sachs, N.; Sonnenberg, A. Cell-Matrix Adhesion of Podocytes in Physiology and Disease. *Nat. Rev. Nephrol.* **2013**, *9*, 200–210. [[CrossRef](#)]
- Greka, A.; Mundel, P. Cell Biology and Pathology of Podocytes. *Annu. Rev. Physiol.* **2012**, *74*, 299–323. [[CrossRef](#)]
- Nagata, M. Podocyte Injury and Its Consequences. *Kidney Int.* **2016**, *89*, 1221–1230. [[CrossRef](#)]

21. Inagaki, M.; Katsumoto, T.; Nanba, E.; Ohno, K.; Suehiro, S.; Takeshita, K. Lysosomal Glycosphingolipid Storage in Chloroquine-Induced α -Galactosidase-Deficient Human Endothelial Cells with Transformation by Simian Virus 40: In Vitro Model of Fabry Disease. *Acta Neuropathol.* **1993**, *85*, 272–279. [[CrossRef](#)]
22. Gregório, P.C.; da Cunha, R.S.; Biagini, G.; Bosquetti, B.; Budag, J.; Ortiz, A.; Sánchez-Niño, M.D.; Barreto, F.C.; Stinghen, A.E.M. Chloroquine May Induce Endothelial Injury through Lysosomal Dysfunction and Oxidative Stress. *Toxicol. Appl. Pharmacol.* **2021**, *414*, 115412. [[CrossRef](#)] [[PubMed](#)]
23. Seydelmann, N.; Wanner, C.; Störk, S.; Ertl, G.; Weidemann, F. Fabry Disease and the Heart. *Best Pract. Res. Clin. Endocrinol. Metab.* **2015**, *29*, 195–204. [[CrossRef](#)] [[PubMed](#)]
24. Turkmen, K.; Guclu, A.; Sahin, G.; Kocyigit, I.; Demirtas, L.; Erdur, F.M.; Sengül, E.; Ozkan, O.; Emre, H.; Turgut, F.; et al. The Prevalence of Fabry Disease in Patients with Chronic Kidney Disease in Turkey: The TURKFAB Study. *Kidney Blood Press Res.* **2016**, *41*, 1016–1024. [[CrossRef](#)] [[PubMed](#)]
25. Kang, Y.; Law, H.K.W.; Zhang, Y.; Wu, Y.; Zhu, G.H.; Saleem, M.A.; Huang, W.Y. TMT-Based Proteomic Analysis Reveals the Effects of Chloroquine on Human Podocytes. *Am. J. Transl. Res.* **2020**, *12*, 4290–4301. [[PubMed](#)]
26. Mundel, P.; Kriz, W. Structure and Function of Podocytes: An Update. *Anat. Embryol.* **1995**, *192*, 385–397. [[CrossRef](#)] [[PubMed](#)]
27. Perico, L.; Conti, S.; Benigni, A.; Remuzzi, G. Podocyte-Actin Dynamics in Health and Disease. *Nat. Rev. Nephrol.* **2016**, *12*, 692–710. [[CrossRef](#)]
28. Baraldi, A.; Furci, L.; Zambruno, G.; Rubbiani, E.; Annessi, G.; Lusvardi, E. Very Late Activation-3 Integrin Is the Dominant B1-Integrin on the Glomerular Capillary Wall: An Immunofluorescence Study in Nephrotic Syndrome. *Nephron* **1992**, *62*, 382–388. [[CrossRef](#)]
29. Toyoda, M.; Najafian, B.; Kim, Y.; Caramori, M.L.; Mauer, M. Endothelial Fenestration in Human Type 1 Diabetic. *Diabetes* **2007**, *56*, 2155–2160. [[CrossRef](#)]
30. Weil, E.J.; Lemley, K.V.; Mason, C.C.; Yee, B.; Jones, L.I.; Blouch, K.; Lovato, T.; Richardson, M.; Myers, B.D.; Nelson, R.G. Podocyte Detachment and Reduced Glomerular Capillary Endothelial Fenestration Promote Kidney Disease in Type 2 Diabetic Nephropathy. *Kidney Int.* **2012**, *82*, 1010–1017. [[CrossRef](#)]
31. Han, S.Y.; Kang, Y.S.; Jee, Y.H.; Han, K.H.; Cha, D.R.; Kang, S.W.; Han, D.S. High Glucose and Angiotensin II Increase B1 Integrin and Integrin-Linked Kinase Synthesis in Cultured Mouse Podocytes. *Cell Tissue Res.* **2006**, *323*, 321–332. [[CrossRef](#)] [[PubMed](#)]
32. Sawada, K.; Toyoda, M.; Kaneyama, N.; Shiraiwa, S.; Moriya, H.; Miyatake, H.; Tanaka, E.; Yamamoto, N.; Miyauchi, M.; Kimura, M.; et al. Upregulation of α 3 β 1-Integrin in Podocytes in Early-Stage Diabetic Nephropathy. *J. Diabetes Res.* **2016**, *2016*, 1–7. [[CrossRef](#)] [[PubMed](#)]
33. Kreidberg, J.A.; Donovan, M.J.; Goldstein, S.L.; Rennke, H.; Shepherd, K.; Jones, R.C.; Jaenisch, R. Alpha 3 Beta 1 Integrin Has a Crucial Role in Kidney and Lung Organogenesis. *Development* **1996**, *122*, 3537–3547. [[CrossRef](#)]
34. Sachs, N.; Kreft, M.; Van Den Bergh Weerman, M.A.; Beynon, A.J.; Peters, T.A.; Weening, J.J.; Sonnenberg, A. Kidney Failure in Mice Lacking the Tetraspanin CD151. *J. Cell Biol.* **2006**, *175*, 33–39. [[CrossRef](#)]
35. Chen, J.; Gui, D.; Chen, Y.; Mou, L.; Liu, Y.; Huang, J. Astragaloside IV Improves High Glucose-Induced Podocyte Adhesion Dysfunction via A3 β 1 Integrin Upregulation and Integrin-Linked Kinase Inhibition. *Biochem. Pharmacol.* **2008**, *76*, 796–804. [[CrossRef](#)] [[PubMed](#)]
36. Dessapt, C.; Baradez, M.O.; Hayward, A.; Dei Cas, A.; Thomas, S.M.; Viberti, G.; Gnudi, L. Mechanical Forces and TGF β 1 Reduce Podocyte Adhesion through A3 β 1 Integrin Downregulation. *Nephrol. Dial. Transplant.* **2009**, *24*, 2645–2655. [[CrossRef](#)]
37. Reiser, J.; Oh, J.; Shirato, I.; Asanuma, K.; Hug, A.; Mundel, T.M.; Honey, K.; Ishidoh, K.; Kominami, E.; Kreidberg, J.A.; et al. Podocyte Migration during Nephrotic Syndrome Requires a Coordinated Interplay between Cathepsin L and A3 Integrin. *J. Biol. Chem.* **2004**, *279*, 34827–34832. [[CrossRef](#)]
38. Fujino, T.; Hasebe, N. Alteration of Histone H3K4 Methylation in Glomerular Podocytes Associated with Proteinuria in Patients with Membranous Nephropathy. *BMC Nephrol.* **2016**, *17*, 1–15. [[CrossRef](#)]
39. Schiwiek, D.; Endlich, N.; Holzman, L.; Holthöfer, H.; Kriz, W.; Endlich, K. Stable Expression of Nephrin and Localization to Cell-Cell Contacts in Novel Murine Podocyte Cell Lines. *Kidney Int.* **2004**, *66*, 91–101. [[CrossRef](#)]
40. Mosmann, T. Rapid Colorimetric Assay for Cellular Growth and Survival: Application to Proliferation and Cytotoxicity Assays. *J. Immunol. Methods* **1983**, *65*, 55–63. [[CrossRef](#)]
41. Repetto, G.; del Peso, A.; Zurita, J.L. Neutral Red Uptake Assay for the Estimation of Cell Viability/ Cytotoxicity. *Nat. Protoc.* **2008**, *3*, 1125–1131. [[CrossRef](#)] [[PubMed](#)]

Disclaimer/Publisher’s Note: The statements, opinions and data contained in all publications are solely those of the individual author(s) and contributor(s) and not of MDPI and/or the editor(s). MDPI and/or the editor(s) disclaim responsibility for any injury to people or property resulting from any ideas, methods, instructions or products referred to in the content.